

1 The Liquid Argon Purity Demonstrator

2 M. Adamowski^a, B. Carls^a, E. Dvorak^b, A. Hahn^a, W. Jaskierny^a, C. Johnson^a, H. Jostlein^a,
3 C. Kendziora^a, S. Lockwitz^a, B. Pahlka^{a*}, R. Plunkett^a, S. Pordes^a, B. Rebel^a, R. Schmitt^a,
4 M. Stancari^a, T. Tope^{a†}, E. Voirin^a, T. Yang^a

5 ^aFermi National Accelerator Laboratory, P.O. Box 500, Batavia, IL, 60510, USA

6 ^bSouth Dakota School of Mines & Technology, 501 East Saint Joseph Street, Rapid City, SD
7 57701, USA

8 **ABSTRACT**

9 The Liquid Argon Purity Demonstrator was an R&D test stand designed to determine if
10 electron drift lifetimes adequate for large neutrino detectors could be achieved without first
11 evacuating the cryostat. We describe here the cryogenic system, its operations, and the appa-
12 ratus used to determine the contaminant levels in the argon and to measure the electron drift
13 lifetime. The liquid purity obtained by this system was facilitated by replacing the evacua-
14 tion step with a filtered gas purge and by minimizing the gaseous impurities from the ullage
15 re-entering the liquid at the gas-liquid interface by first condensing and filtering the gas before
16 returning to the cryostat. The measured electron drift lifetime in this test was greater than 5
17 ms, sustained over several periods of many weeks. Measurements of the temperature profile in
18 the argon were also made and are compared to simulation.

19 **1. Introduction**

20 Liquid argon (LAr) time projection chambers (TPCs) provide a robust and elegant method
21 for measuring the properties of neutrino interactions above a few tens of MeV by providing
22 3D event imaging with excellent spatial resolution. The ionization electrons created by the
23 passage of charged particles through the liquid are transported with typical diffusion of less
24 than a millimeter by a uniform electric field over macroscopic distances. Imaging is achieved by
25 sets of parallel wires oriented in different directions and perpendicular to the drift field. The
26 signals induced by the drifting electrons on the wires are amplified and digitized by wave-form
27 recording electronics. The projection of a particle track in the plane perpendicular to the drift
28 field, i.e. the plane of the wires, is given by the pattern of hits on the wire planes while the
29 projection of the track in the plane parallel to the wires is given by the arrival time of the
30 signals on the wires [1,2]. This technology requires that electrons drift without attachment to
31 electronegative contaminants. LArTPC technology has experienced renewed and strengthened
32 interest since having recently been chosen as the preferred technology for the LBNE future
33 long-baseline neutrino oscillation experiment [3]. We begin with a brief overview of LArTPC
34 development.

35 The ICARUS Collaboration led a pioneering effort in the development of LArTPC technology
36 culminating in the construction of the T600 LArTPC in 2001 [4]. The T600 LArTPC is housed
37 in a 760 ton capacity cryostat that is surrounded by insulating layers of Nomex honeycomb

*Corresponding author: pahlka@fnal.gov (B. Pahlka)

†Corresponding author: tope@fnal.gov (T. Tope)

1 cells [5]. The cryostat was evacuated to a pressure of 10^{-4} mbar before filling with liquid argon.
 2 Electron lifetimes greater than 6 ms were obtained with a contamination less than 50 parts per
 3 trillion (ppt) oxygen equivalent.

4 The Materials Test Stand (MTS) at the Fermi National Accelerator Laboratory (Fermilab)
 5 was developed to evaluate the effect of different materials on electron lifetime [6]. The system
 6 uses a 250 L vacuum-insulated vessel that was evacuated to a pressure of 10^{-6} Torr before filling.
 7 The system employed commercial filter materials in a Fermilab-designed filter system to reduce
 8 contamination from water and oxygen and measured electron lifetimes of approximately 8 ms
 9 using a dedicated purity monitor.

10 The ArgoNeuT project at Fermilab was the first LArTPC in The United States to be placed
 11 in a neutrino beam [7]. Commissioned in 2009, it had an 550 L vacuum insulated cryostat that
 12 was evacuated before filling with liquid argon. The purification system only purified re-liquefied
 13 argon gas boiled off in the gaseous region of the cryostat. With this system, ArgoNeuT was able
 14 to obtain lifetimes of about 750 μ s.

15 The ARGONTUBE LArTPC of AEC-LHEP University of Bern was developed to investigate
 16 the ability to drift electrons over distances of up to 5 m [8]. It uses a vacuum insulated cryostat
 17 and is evacuated to 5×10^{-5} mbar before filling with liquid argon. ARGONTUBE has been able
 18 to reach contamination levels down to 0.15 parts per billion and achieved lifetimes of 2 ms with
 19 a 240 V/cm drift field.

20 The conventional liquid argon vessels described in this section were evacuated to remove water,
 21 oxygen, and nitrogen contaminants present in the ambient air prior to filling with liquid argon.
 22 However, physics requirements for long-baseline neutrino experiments dictate larger cryogenic
 23 vessels to hold bigger detectors and the mechanical strength required to resist the external
 24 pressure of evacuation becomes prohibitively costly. Thus, the concept of purification without
 25 evacuation and testing with The Liquid Argon Purity Demonstrator (LAPD) was proposed in
 26 2006 [9].

27 The LAPD located at Fermilab was designed to achieve the ultra high purity required by
 28 LArTPCs in a vessel that cannot be evacuated. The system relies heavily on the experience
 29 from the MTS [6] in its design and operation plan. Argon purification proceeded in three stages.
 30 Electron drift lifetimes are measured through a sequence of steps as follows. Previous studies
 31 suggest that the concentration of oxygen in a vessel purged with gaseous argon can be reduced
 32 to 100 ppm after 2.6 volume exchanges [10]. Thus, prior to filling with liquid argon, ambient air
 33 in the cryostat is removed by purging the tank with argon gas.

34 After the initial purge, once the water and oxygen concentrations are at the level of a few
 35 ppm, the walls of the cryostat are heated to dry the surfaces and the argon gas is subsequently
 36 circulated through filter vessels to further reduce these contaminants. Liquid argon is then
 37 introduced into the vessel after impurity concentrations less than 1 ppm are achieved. The liquid
 38 is then continuously circulated through the filter vessels in order to achieve concentrations of
 39 water and oxygen on the order of 0.1 parts per billion (ppb). A photograph and a 3D rendering
 40 of the LAPD vessel and piping configuration is shown in Figure 1.

41 The LAPD had several secondary goals. First, we studied the number of liquid argon volume
 42 exchanges necessary to achieve drift distances on the scale of 2.5 meters. Second, we compared
 43 simulations of liquid argon temperature gradients and impurity concentrations in the cryostat to
 44 our measurements using dedicated instruments installed in the cryostat. Third, we monitored
 45 and evaluated filter capacity performance as a function of flow rate. Finally, after achieving
 46 the required electron drift lifetimes, the LAPD cryostat was emptied and a TPC of 2 m drift
 47 distance was installed in the central cryostat region. High liquid argon purity was achieved with
 48 the TPC in the tank and the details of these results will be presented in a forthcoming paper.

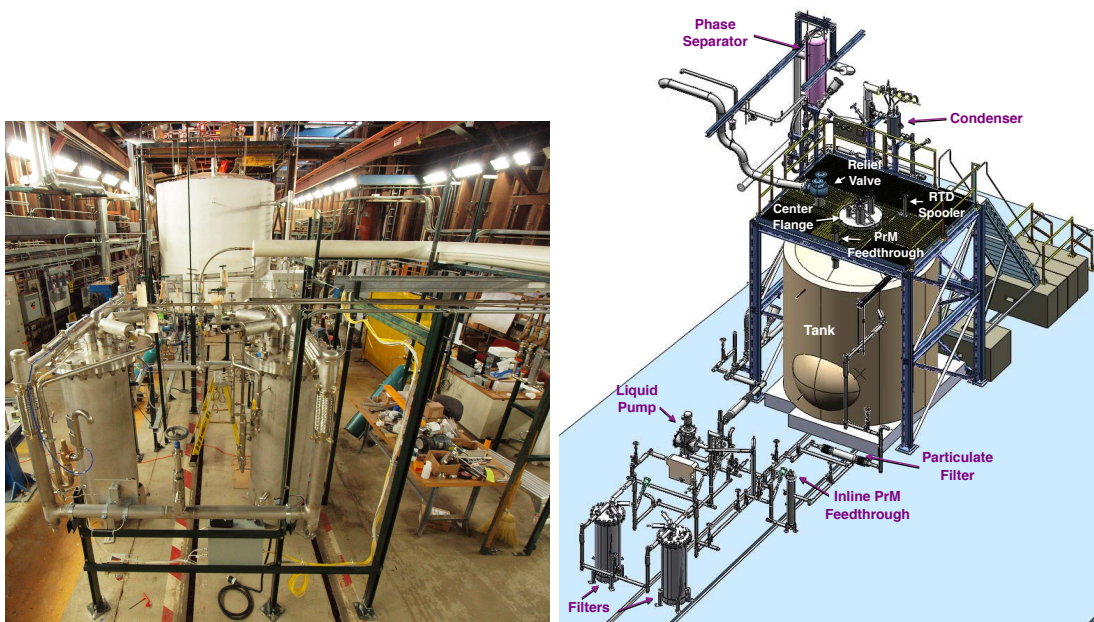


Figure 1. A photograph of the Liquid Argon Purity Demonstration (LAPD) at Fermilab (left) and 3D model of the system (right).

1 2. The Cryostat

2 The LAPD cryostat is an industrial low pressure storage tank. The cryostat has a flat bottom,
 3 cylindrical sides, and a dished head. The cryostat diameter is 3.0 m and the cylindrical walls
 4 have a 3.0 m height. The cryostat is fabricated from 3/16 inch-thick SA-240 stainless steel. The
 5 internal and external (vacuum) maximum allowable working pressures are 3 psig and 0.2 psig,
 6 respectively. Eight perimeter anchors tie the cryostat bottom to the ground to prevent cryostat
 7 uplift. The cryostat volume is 24,628 liters of which 21,210 liters is liquid (29.7 tons) with a
 8 corresponding liquid depth of 2.9 m. Fabrication followed The American Petroleum Institute
 9 Standard 620 Appendix Q as closely as possible and the cryostat welds were fully radiographed.
 10 The cryostat is located inside the Proton Center 4 (PC4) building at Fermilab. Figure 2 shows
 11 a photograph of the LAPD cryostat.

12 The head of the cryostat is populated with four ConFlat flanges and a 76 cm diameter center
 13 flange sealed with an indium wire. Metallic seals are used to prevent the diffusion of contami-
 14 nation that would occur through non-metallic seals. The center flange allows for cryostat entry
 15 using an extension ladder. Five ConFlat flanges populate the center flange, each of which sit
 16 atop stainless steel tube risers such that the flanges remain at room temperature when the
 17 cryostat is cold. Figure 3 shows the layout at the top of the cryostat. At ground level a 76
 18 cm diameter welded manhole is available and intended to make access easier for extended work
 19 inside the cryostat. Table 1 lists the cryostat operating parameters including the heat leak,
 20 volume, operating pressure, and nominal pump flow rates.

21 The cryostat sides and top are insulated with 25 cm of fiberglass which is covered by an outer
 22 layer of 2 cm-thick-foam. The foam is covered with glass cloth and a layer of mastic which
 23 provides a vapor barrier. The cryostat sits on an insulating structural foam base also sealed
 24 with a mastic vapor barrier. The cryostat heat leak was estimated to be approximately 2100



Figure 2. LAPD cryostat sitting on an insulating foam base in PC4. Insulating foam was added to the sides and head later.

Cryostat heat leak	2100 W
Internal max. pressure	3 psig
External max. pressure	0.2 psig
Cryostat volume	24628 liters
Liquid argon volume	21210 liters
Depth at full capacity	2.9 m
Condenser cooling capacity	8400 W

Table 1

The nominal operating parameters for the LAPD including the heat leak, operating pressures, cryostat volume, and condenser cooling capacity.

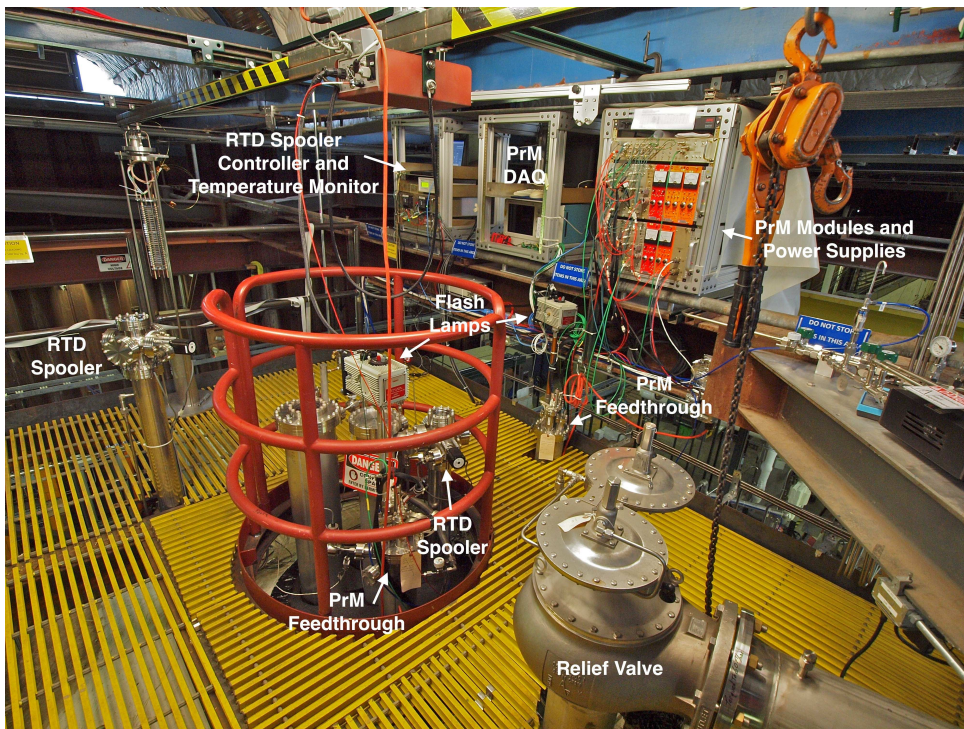


Figure 3. A photograph of the platform on top of the cryostat showing the control systems (see Section 3.5), the RTD translators (see Section 4.1), and the purity monitor feedthroughs (see Section 4.2).

1 W. Natural air flow under the rail cars and cribbing eliminates the need for foundation heaters.
2 The cryostat was cleaned with deionized water and detergent then dried with lint free rags
3 by the cryostat fabricator prior to shipment to Fermilab. After installation of all components
4 at Fermilab, the cryostat was vacuumed with a HEPA filter equipped vacuum. After vacuum
5 cleaning, all walls were wiped with deionized water and lint free rags.

6 **3. The Cryogenics**

7 **3.1. Phase Separator and Condenser**

8 The argon vapor generated by ambient heat input is condensed using liquid nitrogen. A 4,000
9 gallon trailer supplies liquid nitrogen through foam-insulated 2.54 cm Type K copper piping. A
10 phase separator operating at 15 psig near the LAPD cryostat vents nitrogen vapor generated
11 in the nitrogen transfer line so that the condenser is supplied with single phase liquid nitrogen.
12 The phase separator and condenser were designed at Fermilab. A control valve feeding the phase
13 separator maintains a constant liquid level in the phase separator. The condenser consists of
14 an argon volume containing three differently sized coils of tubing through which liquid nitrogen
15 flows. The coiled nitrogen tubing is seamless and all nitrogen connections and welds are outside
16 the condenser to mitigate any nitrogen leak into the LAPD cryostat. Argon vapor is condensed
17 by the liquid nitrogen flowing through the coils.

18 Water outgassing from the tank walls, devices, and cables above the liquid is mixed with argon
19 vapor which needs to be removed to maintain high liquid argon purity. Thus, by default the
20 condensed liquid argon returns to the liquid recirculation pump suction before going through
21 the filters during liquid recirculation. When the pump is off, the condensed liquid argon returns
22 directly to the tank. A control valve feeds the condenser and adjusts the flow to maintain a
23 constant vapor pressure in the ullage. Solenoid valves choose which combination of coils receives
24 liquid nitrogen. The coils operate at near ambient pressure due to the pressure drop across the
25 inlet control valve. The coils will therefore be covered in a thin layer of argon ice due to the
26 large temperature gradient. Argon ice formation was accounted for in the condenser design and
27 no noticeable impact on the cooling due to the argon ice was observed. Vaporized nitrogen is
28 vented outside the enclosure and not recovered. Figure 4 shows a sketch of the condenser design
29 and Figure 5 shows a photo of the phase separator and condenser in PC4.

30 **3.2. Filters**

31 The purification system contains two filters which have identically sized filtration beds of 77
32 liters. The first filter that the process stream enters contains a 4A molecular sieve supplied
33 by Sigma-Aldrich [14] which primarily removes water contamination but can also remove small
34 amounts of nitrogen and oxygen. The second filter contains BASF CU-0226 S, a highly dispersed
35 copper oxide impregnated on a high surface area alumina to remove oxygen [15] and to a lesser
36 extent, water. Thus, the oxygen filter is placed downstream of the molecular sieve to maximize
37 oxygen filtration. The filters are insulated with vacuum jackets and aluminum radiation shields.
38 Metallic radiation shields were chosen because the filter regeneration temperatures would damage
39 traditional aluminized mylar insulation. Piping supplying the filter regeneration gas is insulated
40 both inside the filter vacuum insulation space and outside the filter with Pyrogel XT which is
41 an aerogel based insulation [16] which can withstand temperatures up to 1200 F. Figure 6 shows
42 a 3D rendering of the filter vessel.

43 The filters are regenerated in place using heated gas, which differs from the procedure per-
44 formed by ICARUS [5]. Both LAPD filters are regenerated using a flow of argon gas that is
45 heated to 200°C, supplied by commercial 180 liter liquid argon dewars. Once at 200°C, a small
46 flow of hydrogen is mixed into the primary argon flow and exothermically combines with oxy-
47 gen captured by the filter to create water. Too much hydrogen induces temperatures that are

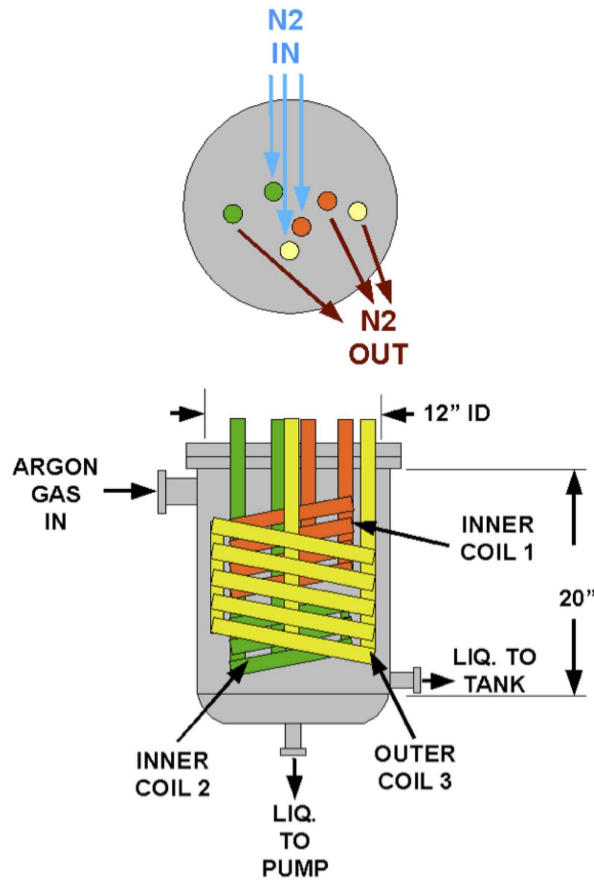


Figure 4. A sketch of the LAPD condenser which shows the three coils of tubing for liquid nitrogen, the inlet for gaseous argon and two outlets for liquefied argon.



Figure 5. A photograph of the LAPD phase separator and condenser. The argon vapor path to the condenser and the two liquefied argon return paths are shown.

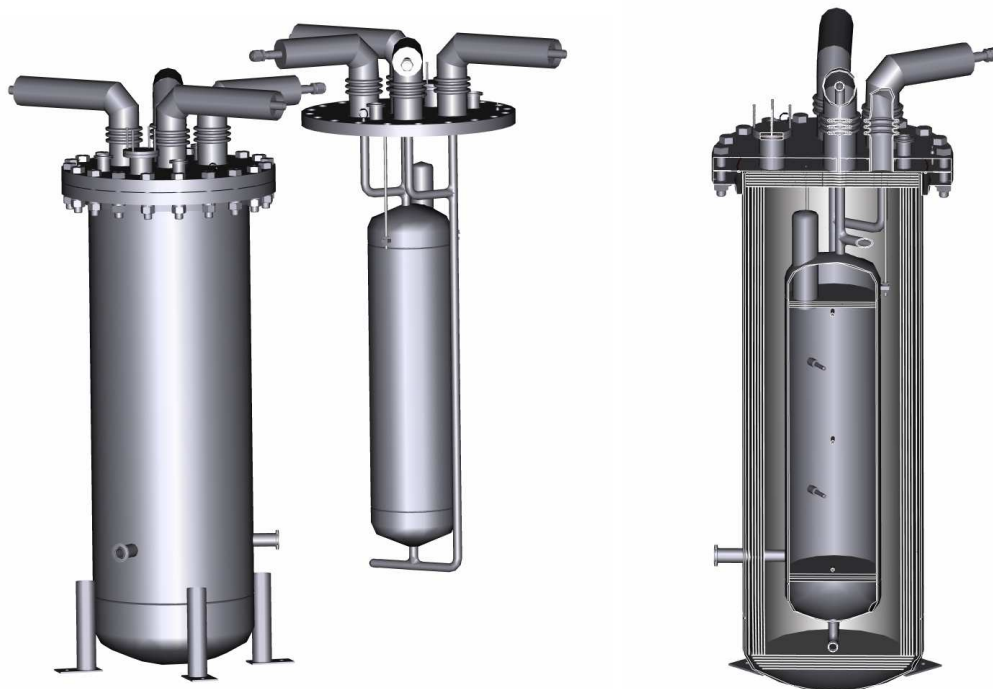


Figure 6. A 3D rendering of the filter vessel. The evacuation vessel and the canister holding the filter material are shown on the left. The cross section of the vessel is shown on the right.

1 sufficiently high to damage the filter. The damage is induced by sintering of the copper which
2 reduces the available filter surface area. Thus, precautions are taken to maintain a hydrogen
3 fraction below 2.5% of the heated gas mixture. During the heated gas regeneration, five filter
4 bed temperature sensors monitor the filter material temperature and the water content of the
5 regeneration exhaust gas is measured. Both filters are evacuated using turbomolecular vacuum
6 pumps while they cool to remove remaining trace amounts of water.

7 At the filtered liquid return to the tank, a particulate filter with an effective filtration of 10
8 microns protects the tank from any debris in the piping. The filter consists of a commercial
9 stainless steel sintered metal cylinder mounted in a custom cryogenic housing and vacuum jacket.
10 Filtration is accomplished by flowing liquid argon to the interior, then outward through the walls,
11 of the sintered metal cylinder. Flanges on the argon piping, along with flanges and edge welded
12 bellows on the vacuum jacket, allow removal of the particulate filter.

13 3.3. Piping and Valves

14 The schedule 10 stainless steel purification piping that supplies argon to the filters is vacuum
15 jacketed. The inner line containing argon is 2.54 cm in diameter with a 7.62 cm diameter vacuum
16 jacket, except at the pump suction where the inner line is 5.1 cm in diameter with a 12.7 cm
17 diameter vacuum jacket. During the fabrication process, all piping was washed with deionized
18 water and detergent to remove oil and grease then cleaned with ethanol. All valves associated
19 with the argon purification piping utilize a metal seal with respect to ambient air either through
20 a bellows or a diaphragm to prevent the diffusion of oxygen and water contamination. The
21 exhaust side of all relief valves are continuously purged with argon gas to prevent diffusion of
22 oxygen and water from ambient air across the o-ring seal. Where possible, ConFlat flanges with
23 copper seals are used on both cryogenic and room temperature argon piping. Pipe flanges in
24 the system are sealed using spiral wound graphite gaskets. Smaller connections are made with
25 VCR fittings with stainless steel gaskets.

26 3.4. Recirculation Pump

27 The liquid argon pump is a Barber-Nichols [17] BNCP-32B-000 magnetically driven partial
28 emission centrifugal pump which isolates the pump and liquid argon from the electric motor.
29 The impeller, inducer, and driving section of the magnetic coupling each have their own bearings
30 that are lubricated by the liquid argon at the impeller end. The motor is controlled by a variable
31 frequency drive (VFD) which allows adjustment of the pump speed to produce the desired head
32 and flow within the available power range of the motor.

33 The liquid argon flow rate is measured at the pump discharge by an Emerson Process Manage-
34 ment Micro Motion Coriolis flow meter [18]. This flow meter is appropriate for ultra high purity
35 liquid argon because, from the perspective of the liquid argon, it only consists of stainless steel
36 pipe and flanges. The inertial effects of the fluid flow through the flow meter pipes is directly
37 proportional to the mass flow of the liquid. The mass flow rate is computed by measuring the
38 difference in the phase vibration between the two ends of the flow pipe. The flow curve of the
39 liquid argon pump with respect to mass flow and pressure is relatively flat, such that pump
40 speed and differential pressure are not good indicators of the mass flow rate. Thus the liquid
41 argon flowmeter is essential instrumentation if the rate of filtration is to be known.

42 3.5. Control System

43 The LAPD cryogenic system is controlled by a Siemens Programmable Logic Controller
44 (PLC) [11]. The PLC reads out the pressure, liquid level, temperature, gas analyzer instru-
45 mentation, and electron lifetime measured by purity monitors. Human-machine interface con-
46 trols are provided through iFIX software [12] running on a PC, which is connected to the PLC
47 through local ethernet. The iFIX software allows entry of temperature and pressure set points

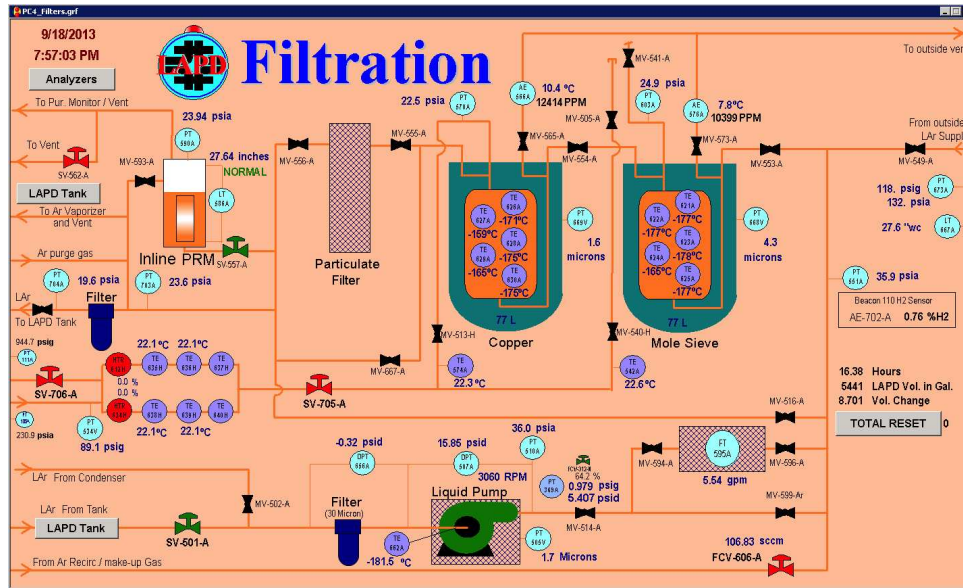


Figure 7. An example of the iFIX graphical user interface for the LAPD controls.

1 and other operational parameters, handles alarming and remote operator controls such as open-
 2 ing and closing valves, displays real-time instrument values, and archives instrument values for
 3 historical viewing. An example of the iFIX graphical user interface used in the LAPD is shown
 4 in Figure 7.

5 4. Cryostat Instrumentation

6 4.1. RTD Translators

7 Two sets of three resistive thermal devices (RTDs) on translators were deployed to measure
 8 thermal gradients in the cryostat at all stages of operation and argon fill level. The motivation
 9 for installing these translators is to verify finite element analysis (FEA) calculations [26] used to
 10 model liquid argon mass flow in the cryostat and to monitor potential convective flow or boiling.

11 One translator is installed near the center of the cryostat and the other is installed 1.0 m
 12 radially outward from the center. Figure 8 shows the locations of the RTD translators inside
 13 the cryostat as well as the purity monitors, discussed in Section 4.2. Each translator consists
 14 of a 50 cm-long circuit board with three RTDs mounted at 22.9 cm intervals, as shown in
 15 Figure 9. The circuit board is suspended at one end of a chain, with a counter-weight at the
 16 other end of the chain to prevent movement during an electrical outage. The chains engage
 17 a 15.13 cm circumference gear that is driven externally, through a ferromagnetic seal, by an
 18 Automation Direct STP-MTRH-23079 stepper motor [13]. The housing around the gear also
 19 includes electrical limit switches to stop the motor when the chain limits are reached. The
 20 stepper motor is controlled by an Automation Direct STP-DRV-4850 stepper drive [13].

21 Teflon ribbon cables connect the circuit boards to a LakeShore model 218 temperature monitor
 22 which reads out all six RTDs. The stepper motor controller and LakeShore are controlled and
 23 read out by a custom LabVIEW application. The RTDs are platinum, type K 100 Ohm and were
 24 measured to be accurate to within 0.5 K. During a typical acquisition, the circuit board translates
 25 vertically through the cryostat and temperature data are acquired at twenty equidistant steps
 26 spanning the cryostat height. Each data point consists of sixty-four single RTD measurements

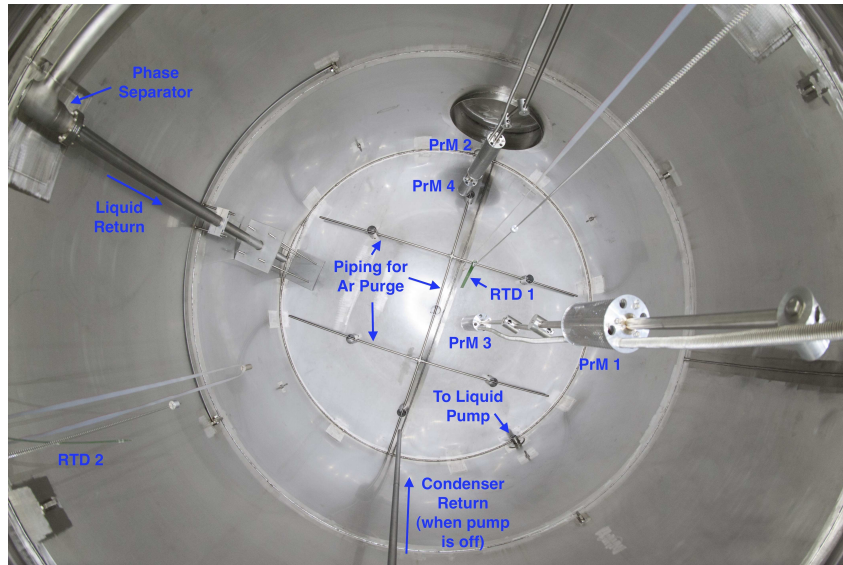


Figure 8. The interior of the cryostat viewed from the top. The purity monitors, RTD translators and piping are shown.

1 with times between steps being long enough to mitigate bias in movement and ensure thermal
 2 equilibrium. Acquisition times between data points are approximately 5 and 30 minutes for
 3 measurements in the liquid and gas, respectively.

4 The liquid argon in the LAPD cryostat is not at thermal equilibrium. The vapor is continually
 5 being removed and condensed in an external condenser, then admixed with liquid argon drawn
 6 directly from the cryostat and then sent through purification filters before being returned to
 7 the cryostat. This evaporation of liquid argon from the surface is seen visually by a surface
 8 turbulence, and detected by the RTDs as a temperature drop between the bulk liquid below the
 9 surface and the vapor above in the ullage.

10 Figure 10 shows a scan of the cryostat taken after the first fill of liquid argon for the central
 11 and peripheral RTD translators. A very sharp temperature gradient, approximately 80 K over
 12 50 cm is present in the ullage just above the liquid surface. The data shown were taken only
 13 from the downward direction to avoid the thermal lag one sees when the circuit board is moving
 14 out of the liquid.

15 Figure 11 shows the temperature measurements for the central RTDs obtained from a rela-
 16 tively quick scan with the cryostat full. The slight change of temperature with depth is less
 17 than 25 mK over 2 m. At the bottom of the scan there is a fluctuation of approximately 30 mK,
 18 attributed to the returning purified liquid argon introduced at the bottom of the cryostat. The
 19 measurement distribution of any one RTD at a given position in the liquid, suggests a peak-to-
 20 peak spread of about 10 mK, implying the relative precision of a single measurement is on the
 21 order of a few mK. The measurements are compared to FEA calculations [26] and show good
 22 agreement in both the gradient and absolute temperature.

23 4.2. Purity Monitors

24 The purity of liquid argon is continuously monitored by a double gridded ion chamber im-
 25 mersed in the liquid argon volume. The fraction of electrons generated at the cathode that
 26 arrive at the anode (Q_A/Q_C) after the electron drift time, t , is a measure of the electronegative



Figure 9. The peripheral RTD translator inside the LAPD cryostat.

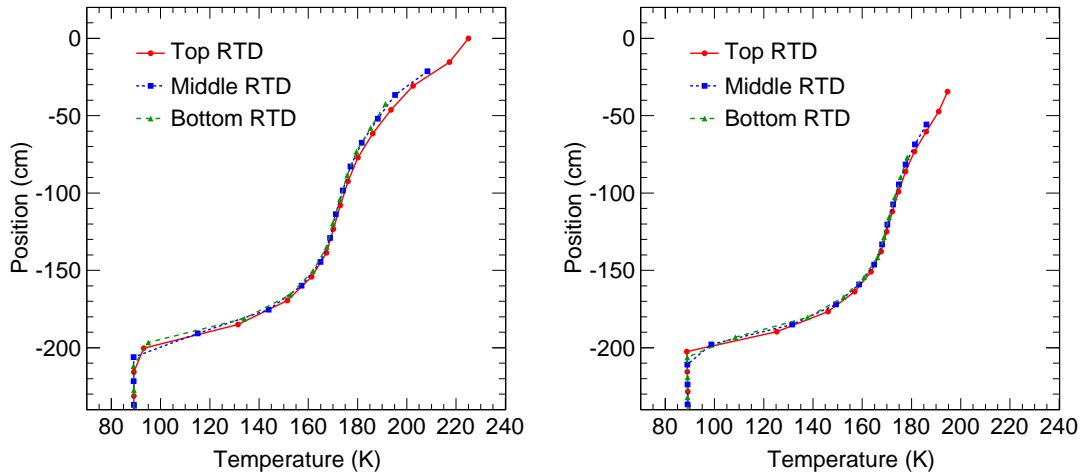


Figure 10. The cryostat temperature as measured by the three central (left) and the three peripheral (right) RTDs. Data were taken after the first trailer of liquid argon was delivered to the cryostat, corresponding to a liquid argon depth of 69 cm. On these Figures, the liquid surface corresponds to a value of 200 cm as measured from the top of the cryostat.

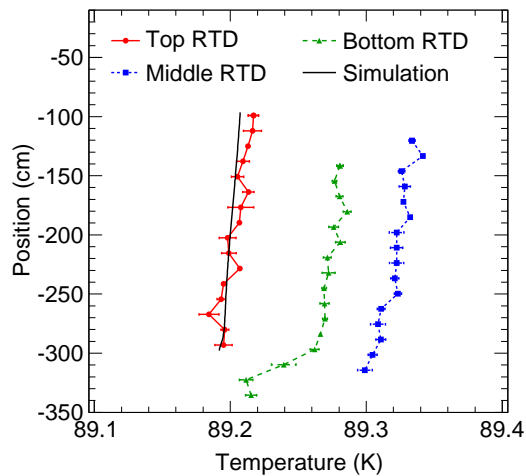


Figure 11. The liquid argon temperature taken at several locations within the cryostat as measured by the three central RTDs, compared to FEA calculations. This figure illustrates the precision with which the temperature is measured and shows a temperature variation of less than 25 mK over 2 m.

1 impurity concentration and can also be interpreted as the electron lifetime, τ such that

$$2 \quad Q_A/Q_C = e^{-t/\tau}. \quad (1)$$

3 4.2.1. Hardware

4 The purity monitor is based on the design described in Reference [24]. It consists of four
5 parallel, circular electrodes: a disk supporting a photocathode, two open wire grids, one anode
6 and one cathode, and an anode disk. The anode disk and photocathode support disk are made
7 of stainless steel; the two grid support rings are made of G-10 circuit board material with the
8 grid wires soldered to the copper clad surface. The region between the anode grid and cathode
9 grid contains a series of field-shaping stainless steel rings. The two grids, each with a single set
10 of parallel wires, are made of electro-formed gold-sheathed tungsten with a 2.0 mm wire spacing,
11 25 μm wire diameter and 98.8% geometrical transparency.

12 The cathode grid is at ground potential. The cathode, anode grid, and anode are electrically
13 accessible via modified vacuum grade high voltage feed-throughs. The anode grid and the field-
14 shaping rings are connected to the cathode grid by an internal chain of 50 M Ω resistors to ensure
15 the uniformity of the electric fields in the drift regions. To ensure maximum transparency [25],
16 the field ratios typically satisfy

$$17 \quad E_1 > 2E_2 > 4E_3 \quad (2)$$

18 where E_1 is the field between the anode grid and the anode, E_2 is the field between the anode
19 grid and the cathode grid, and E_3 is the field between the cathode and the cathode grid.

20 The photocathode is a 2.54 cm \times 3.81 cm \times 0.8 mm aluminum plate, coated with 50 \AA of
21 titanium and 1000 \AA of gold and attached to the cathode disk [19]. A xenon flash lamp [20] is
22 used as the light source. The UV output of the lamp has a wide spectrum above approximately
23 225 nm. An inductive pickup coil on the power leads of the lamp provides a trigger signal
24 when the lamp flashes. Light is directed via three multi-mode quartz optical fibers [21] to the
25 photocathode. Only one fiber is needed; the other two are for redundancy. The fibers have a 0.6
26 mm core diameter and 25.4 degrees of full acceptance cone. The attenuation is 0.95 dB/m at
27 200 nm. The fibers underwent a series of tests using a photodiode read out by an oscilloscope to
28 measure the stability and light output linearity as a function of input light intensity and showed
29 no anomalous behavior.

30 The electrons liberated from the photocathode drift towards the cathode grid and induce a
31 current on the cathode. After crossing the cathode grid, the electrons drift between the two
32 grids. During this time essentially no current is induced on the cathode or anode due to the
33 shielding effect of the grids. After crossing the anode grid, the electrons induce a current on
34 the anode. The signals induced on the cathode and anode are fed into two charge amplifiers in
35 a purity monitor electronics module. The charge amplifiers have a 5 pF integration capacitor
36 with a 22 M Ω resistor in parallel with the capacitor. The signal and high voltage are carried on
37 the same cable and decoupled inside the purity monitor electronics module. Figure 12 shows a
38 schematic of a purity monitor installed in the cryostat.

39 The LAPD system employs five purity monitor units at different locations. Each purity
40 monitor is contained in a stainless steel, perforated Faraday cage to isolate the system from
41 outside electrostatic interference. There are two types of purity monitors with different lengths
42 and different numbers of field-shaping rings: three long purity monitors that are 55 cm in length
43 and two short purity monitors that are 24 cm in length. The operational range of Q_A/Q_C
44 for which a purity monitor can make sensible measurements is about 0.05 - 0.95. Thus, longer
45 electron drift lengths correspond to operational ranges shifted to sample larger electron lifetimes.
46 An assembly of one long purity monitor and one short purity monitor is located vertically along

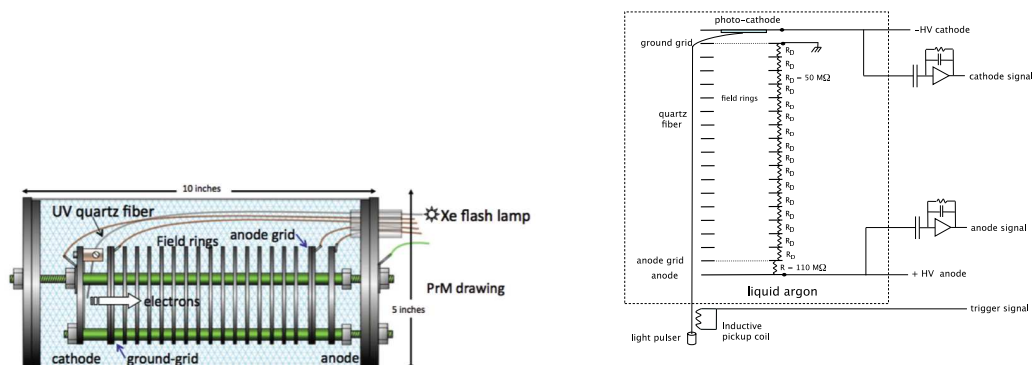


Figure 12. A drawing (left) and schematic (right) of a liquid argon purity monitor employed in LAPD.

1 the central axis of the cryostat. Another identical assembly is located at a distance of 1.1 m
 2 away from the center of the cryostat. Figure 13 shows a photograph of the assembly located
 3 near the cryostat periphery. One long purity monitor, referred to as the inline purity monitor,
 4 is located in the circulation pipe to measure the liquid argon purity before the liquid enters
 5 the cryostat. Three flash lamps are used for the two purity monitor assemblies and the inline
 6 purity monitor. Table 2 shows the geometrical characteristics and voltage settings of the purity
 7 monitors installed in the cryostat.

8 4.2.2. Data Acquisition

9 Measurements of the electron lifetime are taken several times a day using a Fermilab-designed
 10 acquisition program. Each measurement takes about one minute. The flash lamp and the high
 11 voltage to the purity monitors are only powered during this time to protect the flash lamp,
 12 minimize degradation of the quartz fiber and reduce dust/particle accumulation on the purity
 13 monitor photocathode. The automation module will switch off both the flash lamp power supply
 14 and high voltage to the purity monitor if the lamp has been flashing for more than 140 seconds.
 15 An 8-channel analog multiplexing unit (MUX) is used to select which purity monitor signal is
 16 readout. Each channel of the MUX has four inputs, three of which read the cathode and anode
 17 signals from one purity monitor after the amplifiers and the trigger signal from the inductive
 18 pickup coil. Figure 14 shows a block diagram of LAPD purity monitor system.

19 The program initializes and reads out the signals from each purity monitor one by one. When
 20 the flashlamp fires, a large voltage perturbation is induced on the cathode and anode connections
 21 which distorts the shape of the electron signals. This perturbation is measured and recorded
 22 before turning on the high voltage to the purity monitors. The anode and cathode signals from
 23 each purity monitor are then measured by constructing the average of ten waveform samples
 24 per acquisition, each of which are stored for offline analysis. The pulses registered from the
 25 voltage perturbation due to the light source are subtracted from the signal before calculating
 26 the lifetimes. A plot of the averaged and smoothed signal traces produced from a purity monitor,
 27 before and after noise subtraction, is shown in Figure 15.

28 The maximum pulse height, V_{max} , of the anode and cathode traces are identified for each
 29 waveform as the maximum number in the array of numbers that stores the noise-subtracted
 30 digitized waveform. The charge seen by the cathode and anode is then calculated as $Q =$



Figure 13. One assembly of one long purity monitor and one short purity monitor inside LAPD.

Table 2

Geometrical characteristics and voltage settings of the purity monitor. V_{AG} and V_A are the applied voltages on the anode grid and at the anode, respectively. Electric field values are reported for nominal operation.

	Long monitor	Short monitor
Cathode, Anode disk, grid diameter	8 cm	
Cathode-Anode total drift distance	50 cm	19 cm
Cathode grid to Anode grid distance	47 cm	16 cm
Cathode-Cathode Grid gap	1.8 cm	
Anode Grid-Anode gap	0.79 cm	
Number of field-shaping rings	45	15
Number of resistors	46	16
Anode disk/Cathode disk thickness	0.23 cm	
Anode grid/Cathode grid thickness	0.24 cm	
Field-shaping ring thickness	0.23 cm	
Gap between rings	0.79 cm	
Nominal Cathode Voltage	-100 V	-100 V
Nominal Anode Voltage	5 kV	2 kV
V_{AG}/V_A	0.948	0.865
Electric field between cathode grid and cathode	56 V/cm	56 V/cm
Electric field between cathode and anode grids	101 V/cm	108 V/cm
Electric field between anode and anode grid	329 V/cm	342 V/cm

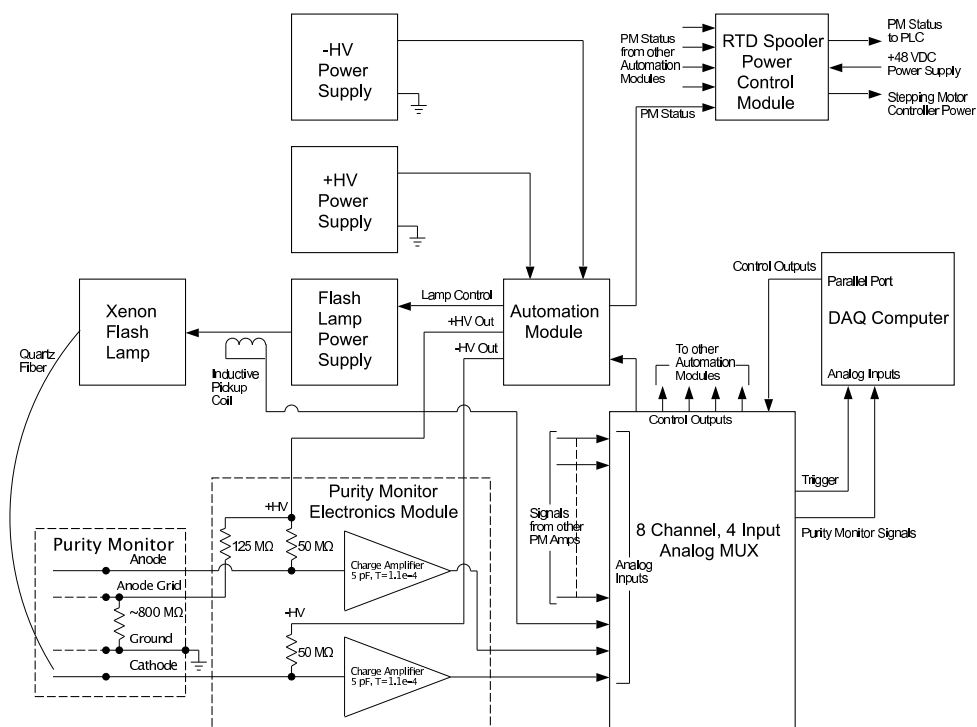


Figure 14. Block diagram of LAPD purity monitor system.

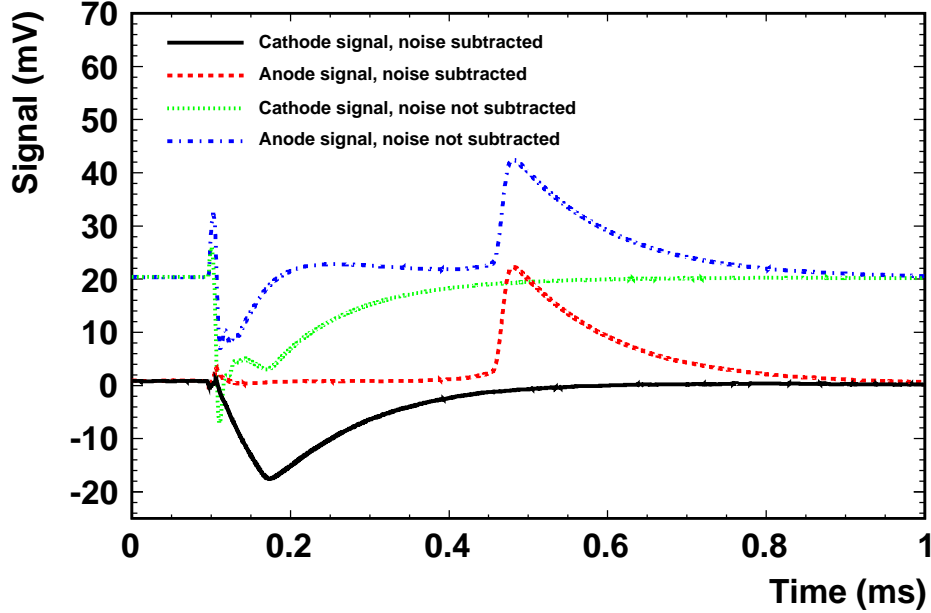


Figure 15. A screenshot of anode and cathode signals before and after noise removal from the digitizer.

1 $(V_{max} - V_0) \times f(\Delta t, RC)$, where V_0 is the measured baseline for the trace and $f(\Delta t, RC)$ is a
 2 correction for the electronics response function that depends on the time duration of the current
 3 pulse, Δt , and the measured RC time constant of the electronics.

4 An additional source of electrical noise that affected the operation of the purity monitor DAQ
 5 was found to be the RTD translator stepper motor controllers. These controllers have a DC
 6 to DC switching converter that provides the holding current to the stepper motors used in the
 7 RTD translator system. The most effective way to mitigate this noise source was to remove
 8 the 48 volt DC bulk power to the stepping motor controllers whenever the purity monitor DAQ
 9 was running. After the purity monitors were turned off by the DAQ, the 48 volt DC power was
 10 restored to the stepping motor controllers and a reset signal was given to the controllers so that
 11 they would index back to the zero starting point for their data collection.

12 4.2.3. Lifetime and Attenuation Corrections

13 The lifetime relies on measurements of the anode voltage, V_A and the cathode voltage, V_C ,
 14 which in turn depend on amplification of induced currents on the anode and cathode. The
 15 potential exists for differences in amplification between the anode and cathode signal voltages
 16 to have an impact on the lifetime. We model the amplification as $V_A = g_\alpha Q_A$ and $V_C = g_\beta Q_C$,
 17 where g_α and g_β are constants. If the two amplifiers used for the anode and cathode signals
 18 are switched, the amplification becomes $V'_A = g_\beta Q_A$ and $V'_C = g_\alpha Q_C$. The primes indicate
 19 measurements taken with the amplifiers for the anode and cathode swapped. The lifetime and
 20 attenuation calculations can then be calibrated by making measurements of V_A , V'_A , V_C , and V'_C

1 using

$$2 \frac{g_\alpha}{g_\beta} = \sqrt{\frac{V_A/V_C}{V'_A/V'_C}}. \quad (3)$$

3 During a span of several days at nearly constant argon purity, measurements were taken
 4 with the amplifiers swapped to measure the ratio g_α/g_β . For the purity monitor with the best
 5 performance, g_α/g_β was measured to be 0.973. With the measurements taken, a correction to
 6 the lifetimes was applied using **why do we use this correction and why is it correct?**

$$7 \tau = \frac{t}{\ln((Q_C/Q_A) \times (g_\alpha/g_\beta))}. \quad (4)$$

8 An additional cross-check was performed by examining the effect of varying the high volt-
 9 age applied to the cathode and anode. Lifetime measurements from a single purity monitor
 10 were taken at anode voltages of 2 kV, 3 kV, 4 kV, and 5 kV. Each study resulted in purity
 11 measurements consistent with those at nominal high voltage.

12 4.2.4. Systematic Uncertainties

13 There are three sources of systematic uncertainty that could be significant. For each of these
 14 quantities, limits were used to determine a lower limit for Q_A/Q_C , so that a lower limit on
 15 the electron drift lifetime can be quoted. The first is the acceptance of the anode, which we
 16 assume to be 100%. It is different from 100% if any electrons generated at the cathode traverse
 17 the entire drift distance without encountering an impurity, but are not counted at the anode
 18 because the travelled too far transversely from the axis of the purity monitor. The second is the
 19 possibility that electrons generated at the cathode induce a signal on the cathode grid, and are
 20 thus counted in Q_C , but were actually absorbed by an impurity before arriving at the cathode
 21 grid. We assume that this does not happen, and thus the value of Q_C used is an upper limit. The
 22 third is the uncertainty on the RC time constant used to correct for the electronics response, as
 23 discussed previously. If any of these quantities is different than assumed, then the actual values
 24 of Q_A/Q_C and the electron drift lifetime are larger than quoted.

25 4.3. Gas Analyzers

26 4.3.1. Oxygen, Water and Nitrogen Monitors

27 LAPD has an extensive gas analysis system to monitor and diagnose the processes that take
 28 the cryostat from atmospheric air to ultra pure liquid argon. The system consists of seven com-
 29 mercial gas analyzers. Four of these analyzers measure the oxygen concentration and together
 30 they span the range from 0.1 ppb to 5000 ppm. These four oxygen analyzers are augmented by
 31 two 0.1-25% oxygen sensors which monitor the purge of the cryostat of air and are described
 32 in Section 4.3.2. Two of these seven gas analyzers measure the water concentration and these
 33 span the range from 0.2 ppb to 20 ppm. Dew point meters installed in series with these water
 34 analyzers extend the measurement range from 20 ppm up to ambient dew points as high as
 35 20,000 ppm water. A nitrogen analyzer completes the array of seven gas analyzers with a range
 36 that spans 0.1 to 100 ppm.

37 The gas analyzers are fed by a local switchyard of 56 diaphragm valves. These valves direct
 38 the gas flow from five primary locations in the system to the seven gas analyzers. A primary
 39 location or utility gas can feed anywhere between none and all of the gas analyzers. The primary
 40 measurement locations are the liquid argon cryostat, with the option of sampling from either the
 41 gas or liquid phases, pump discharge, molecular sieve filter output, oxygen filter output, and the
 42 liquid argon fill connection. In addition to the five primary locations, argon and nitrogen gas

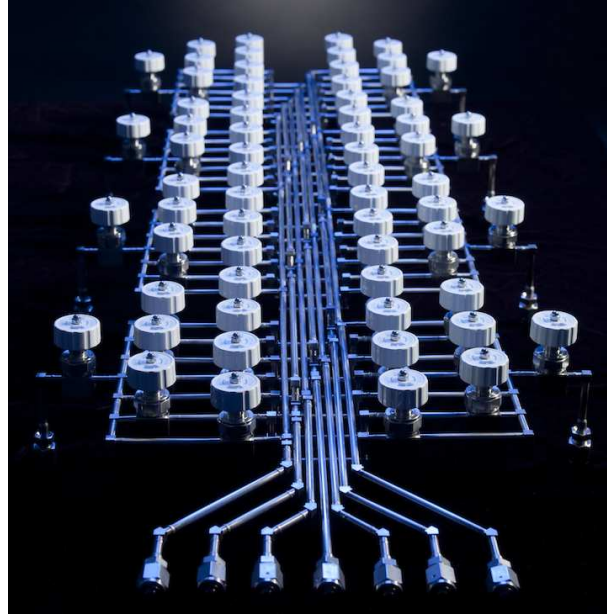


Figure 16. Gas distribution switchyard - liquid argon gas sampling master distribution panel.

1 from utility sources are available to supply analyzers when measurement from a system location
 2 is not required.

3 An oil free vacuum pump is also part of the switchyard and can evacuate the tubing that
 4 connects the measurement locations and the gas analyzers. Evacuation of the sample lines
 5 when switching sample locations greatly reduces the time required to reach equilibrium when
 6 the measured contamination is at the parts per billion concentration. A high purity metal
 7 bellows pump boosts the sample pressure from the 2 psig operating pressure of the liquid argon
 8 cryostat to the 15-20 psig inlet pressure required by the gas analyzers. A photograph of the gas
 9 distribution switchyard is shown in Figure 16.

10 Filter output sampling allows determination of filter performance and capacity. Sampling the
 11 liquid argon fill connection is critical to ensure that the liquid argon supply is within specification.
 12 For example, a trailer of liquid argon was rejected because it was so far out of specification it
 13 would have required an impractical number of filter regenerations to process. Without this
 14 extensive gas analyzer system it would be very difficult to successfully take the cryostat from
 15 ambient air to ultra pure liquid argon.

16 4.3.2. Oxygen Capillary Detectors

17 We deployed thirteen industrial type oxygen sensors, configured in two strings of six and seven,
 18 each consisting of capillary tubes placed at different heights, to measure the oxygen concentration
 19 during the initial gaseous argon purge. One string was placed near the cryostat wall and the
 20 other was placed near the cryostat center. The end of each tube is vertically spaced 76.2 cm
 21 from the next in the string, with the string spanning the height of the cryostat. The central
 22 set was placed on the tank axis, the peripheral set was 112 cm radially out. The sampling tube
 23 inlets were spaced 76.2 cm apart, spanning the height of the tank. The sensors are located inside
 24 small glass jars with plastic coated lids. The sample tubes are 1.6 mm diameter capillaries, and
 25 run continuously from the intake point through a ConFlat flange to the jars. All capillaries

1 are the same length, with the excess length coiled up above the feed-through flange, to assure
2 matched time response. The jars are mounted on feed-through flanges.

3 **5. Results from Operation Modes**

4 The LAPD was operated in two separate run periods. In each period, the cryostat was oper-
5 ated in three phases; a gaseous argon purge, gaseous argon recirculation, and liquid recirculation.
6 The first run period was September 2011 to April 2012. Each of the three phases of operation
7 were performed to test the devices and filters. For this period, the cryostat was filled one-third
8 full to confirm the feasibility of measuring the liquid argon purity. The second period was from
9 December 2012 through October 2013. The cryostat was completely filled with liquid argon and
10 measurements of the liquid argon purity were performed under various operating conditions.
11 This section describes the results for the second period, and when applicable, measurements are
12 compared to those obtained in the first run period.

13 **5.1. Gaseous Argon Purge**

14 A gaseous argon purge was performed at the beginning of each run period. In this phase of
15 operation, gaseous argon is pumped from the bottom of the cryostat displacing the ambient air
16 which exits out the room temperature feedthroughs at the top of the cryostat. This method
17 mimicks an argon “piston” in the sense that the higher density gaseous argon engenders a
18 boundary between it and the ambient air, which moves vertically upwards. For the first period,
19 the two sets of sampling gas capillaries, described in Section 4.3.2, were installed to measure the
20 oxygen concentration and follow the rise of the argon gas as it displaces the lighter ambient air.

21 The purpose of these measurements was to understand the initial levels of impurities and
22 obtain information for comparison to FEA flow models to validate or improve those models.
23 The spatial and temporal concentration measurements provide information about the degree of
24 diffusion and mixing during purges. Each purge lasted approximately 8 volume exchanges or
25 24 hours and corresponds to a 1.15 m/hour piston rise rate and 2.9 and 3.4 hours per volume
26 exchange for the first and second period, respectively. The gaseous argon flow rate was constant
27 throughout each purge. Figure 17 shows the fraction of ambient air retained with respect to
28 the measured oxygen levels during the gaseous argon purge in the first run period for the seven
29 capillary tubes installed in the central region of the cryostat and the six capillary tubes installed
30 in the peripheral region of the cryostat. The front of gaseous argon is clearly present as indicated
31 by the successive reduction of oxygen seen by each capillary tube as a function of time.

32 The capillaries were removed at the end of the first period purge. The removal lasted 15 min-
33 utes, during which time argon gas flowed into the cryostat at 0.14-0.17 cubic meters per minute
34 (m^3/min). During the extraction, the water, oxygen, and nitrogen monitors were switched to
35 argon gas utility as a precaution because the bellows pump drawing gas from the cryostat could
36 pull a vacuum on the cryostat if the argon flow into the cryostat stopped. After these devices
37 were switched back to measuring the cryostat gas, an increase of about 0.2 ppm O_2 and 0.4
38 ppm N_2 was observed. With the capillaries removed, the makeup gas flow dropped from 0.0099
39 m^3/min to 0.0042 m^3/min . At the end of the purge, 203 m^3 had passed through the cryostat,
40 corresponding to 8.2 volume exchanges. The oxygen level was reduced to 5.2 ppm, the water
41 concentration was reduced to 0.99 ppm, and the nitrogen concentration was reduced to 13.4
42 ppm. Figure 18 shows the concentrations of water and oxygen during the gaseous argon purges
43 for both periods, along with the results from the capillary tube oxygen measurements from the
44 first period. In both run periods the water concentration was reduced to approximately 1 ppm.
45 The oxygen concentrations were reduced to 10 and 7 ppm for the first and second run period,
46 respectively. Throughout both purges, the nitrogen concentration remained nominally stable at
47 18 ppm. The argon purges for both run periods delivered similar results.

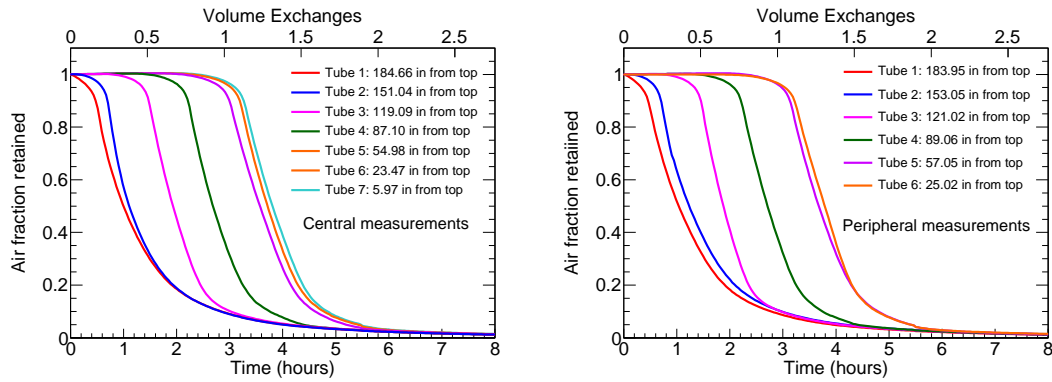


Figure 17. Oxygen concentrations for the a) central and b) peripheral gas sampling capillaries taken at several heights with respect to the cryostat bottom obtained during the initial gaseous argon purge for the first run period.

5.2. Gas Recirculation

After the removal of the ambient air from the argon purge, argon gas was pumped through the molecular sieve and oxygen filter at a rate of a volume exchange every 3.4 hours, then returned to the cryostat. The gas recirculation for the second period ran for about 77 volume exchanges corresponding to one week. Figure 19 shows the oxygen and water concentrations, measured by the water and oxygen gas analyzers, for the gas recirculation phase. At the end of this phase, the oxygen concentration was reduced to approximately 20 ppb and the water concentration reached a stable value of 667 ppb. The nitrogen concentration was reduced to 13.7 ppm. A gap in the data between the 27th and 37th volume exchanges corresponds to a time during which the gas analyzers were sampling alternate components of the system. The overall results for the gas recirculation phase indicate that water outgasses from all surfaces of the cryostat and piping, and that the outgassing rate is matched by the filtration rate after several volume exchanges.

5.3. Liquid Argon Filling

For the second period, the cryostat was filled with liquid argon from the D0 calorimeter at Fermilab. Filling the cryostat occurred in multiple stages. The duration of each fill varied from 4 to 6 hours. Table 3 presents the liquid argon trailer contaminant concentrations along with details of each successive fill for the second run period. The four trailers were delivered over a period of two weeks in January, 2013. The total volume of liquid argon placed in the cryostat was 21,309 liters, corresponding to 29.7 tons.

5.4. Liquid Argon Recirculation

After the cryostat was full, the liquid recirculation pump was started and filtration proceeded by routing liquid argon through the two filters. Figure 20 shows the water and oxygen concentrations in the cryostat liquid as measured by the water and oxygen analyzers as a function of time for three select intervals immediately preceding purity monitor operation. The measured oxygen concentration was compared to simulation assuming perfect mixing in the cryostat (Need explanation for “perfect mixing”). The figure shows that in the first two time intervals, perfect mixing was not achieved. This suggests that the filter efficiency was not sufficient to remove impurities given the initial contamination levels. In the last time interval however, perfect mixing was nearly achieved.

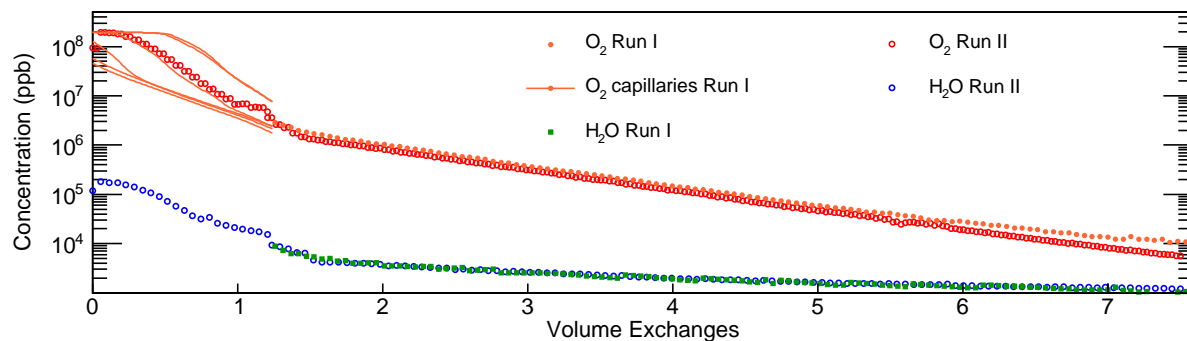


Figure 18. The water and oxygen concentrations in the LAPD during the two gaseous argon purges as a function of the number of volume exchanges. The plot shows the water concentration and the oxygen concentration measured by both the gas analyzer and the oxygen capillary tubes. Similar results were obtained for both purges.

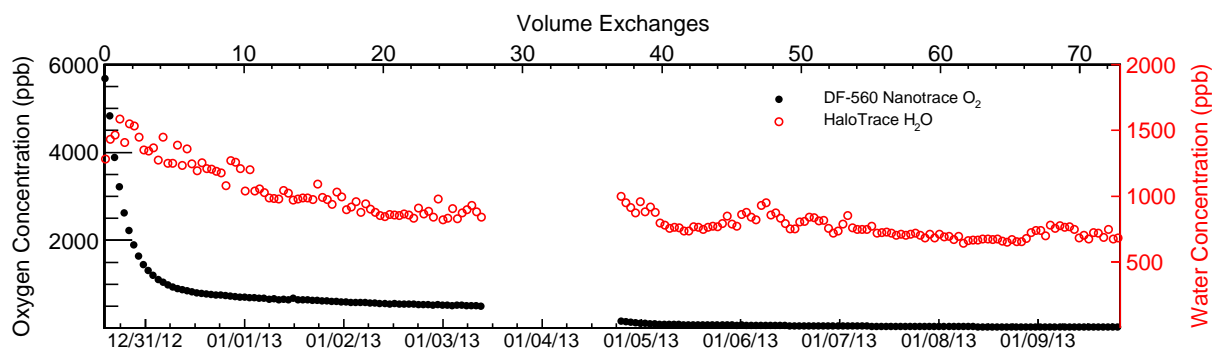


Figure 19. The water and oxygen concentrations in the cryostat gas during the gas recirculation phase of the second period, plotted as a function of time and of the number of volume exchanges.

	O ₂ (ppb)	H ₂ O (ppb)	N ₂ (ppm)	liquid depth (cm)	LPF	Rate (LPM)
Trailer 1	202	99	10	69	5015	1890
Trailer 2	200	225	9	147	10719	2220
Trailer 3	400	180	9	220	16120	1970
Trailer 4	197	66	10	292	21309	1700

Table 3

Concentrations of oxygen, water, and nitrogen measured in each trailer before introduction into LAPD. The liquid argon height is measured in inches from the bottom of the cryostat corresponding to the number of liters delivered to the cryostat in each fill (LPF). Also shown is the fill rate in liters per minute (LPM).

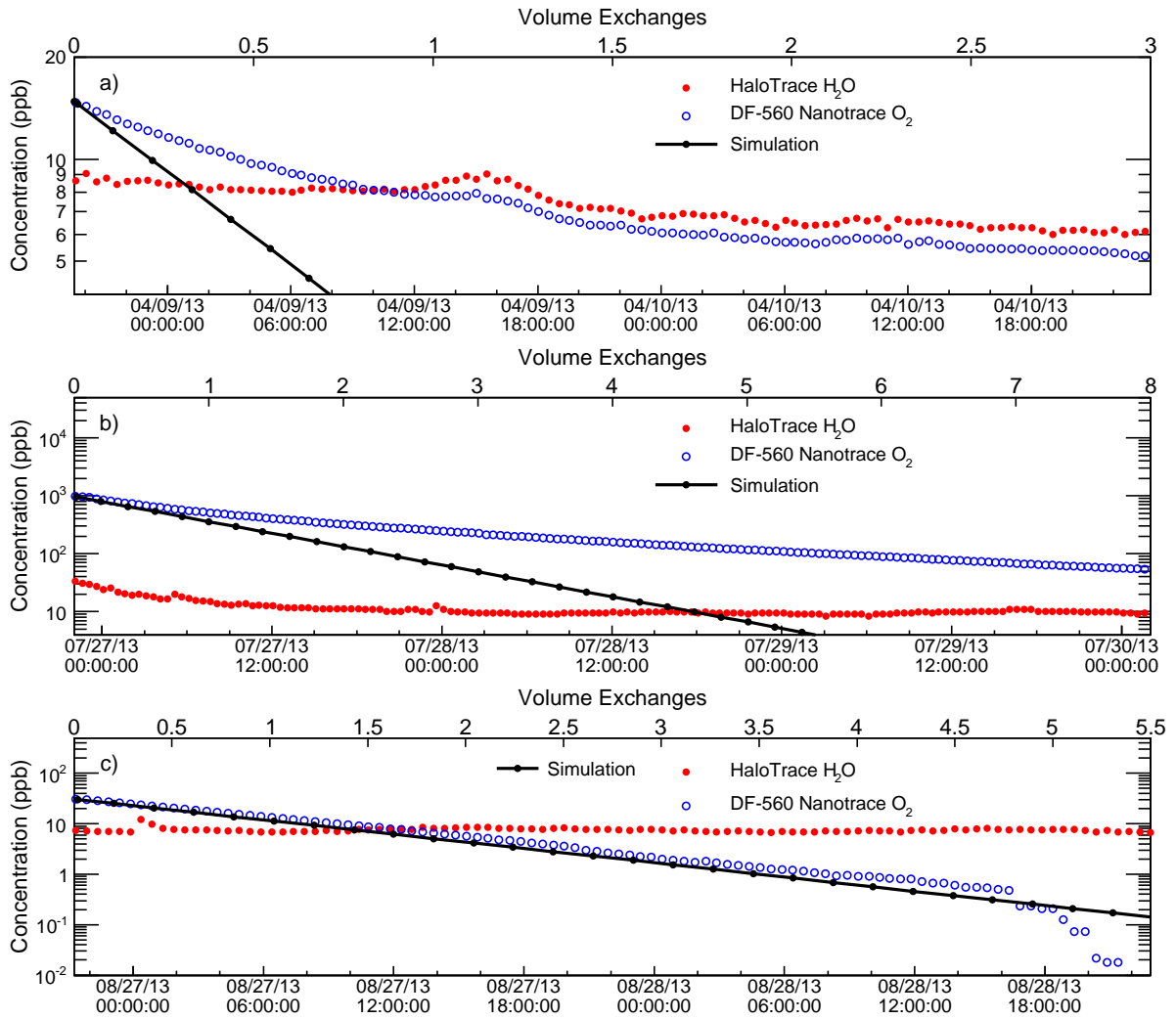


Figure 20. The water and oxygen concentrations in the cryostat liquid for three time intervals before purity monitor operation. The water concentration (solid circles) remained at a constant level of around 10 ppb for each cleanup. The measured oxygen concentration (open circles) is compared to a simulation assuming perfect mixing (black line).

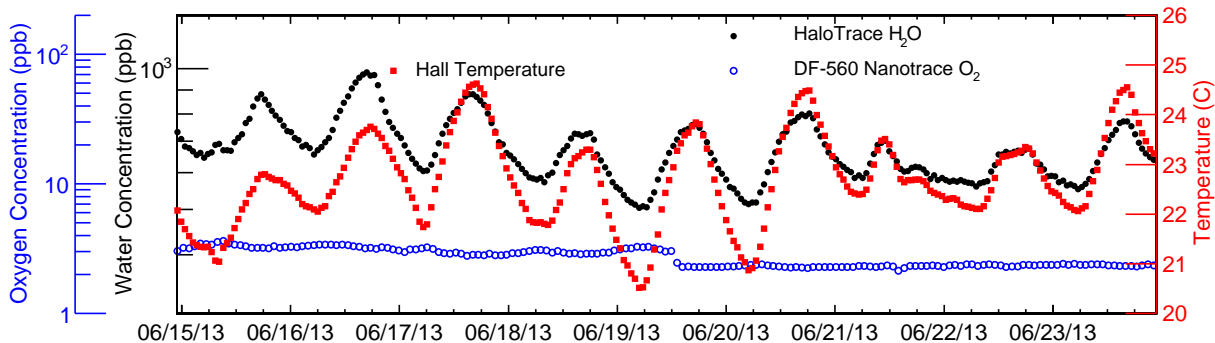


Figure 21. The water concentration (solid circles) and oxygen concentration (open circles) measured in the cryostat vapor space with the cryostat totally filled with liquid argon. Also shown is the temperature in the LAPD hall (solid squares) for the same time period.

1 Figure 21 shows the water and oxygen concentrations measured in the cryostat vapor space
 2 with the cryostat totally filled with liquid argon, along with the temperature in the LAPD
 3 hall. The temperature and the water concentration in the cryostat vapor space are closely
 4 correlated and suggests significant outgassing of water in this region. This is consistent with
 5 results obtained from the MTS and suggests that the majority of the contamination introduced
 6 into the liquid can be attributed to the contamination in the vapor space.

7 After several liquid volume exchanges, the contamination was sufficiently low to begin oper-
 8 ation of the four purity monitors inside the cryostat and the inline purity monitor upstream
 9 from the filters. Figure 22 shows the cathode peak pulse height, Q_C , and the ratio of the an-
 10 ode and cathode peak pulse height, Q_A/Q_C , over the complete LAPD run with several periods
 11 of extended stable running with measured lifetimes of more than 3 ms and occasionally more
 12 than 6 ms. These results were obtained using the short purity monitor located at the periphery
 13 of the tank. Of the five purity monitors, this one showed the best performance and provided
 14 measurements with the highest precision.

15 The cathode purity monitor signal appears to become less efficient over time. Nevertheless,
 16 even with low cathode signals, measured lifetime values are consistent with those at times during
 17 which good signals were achieved. The pump speed, and thus the volume exchange rate were
 18 changed over several time intervals throughout the run. We found no correlation between volume
 19 exchange rate and measured lifetime values.

20 6. Discussion and Conclusion

21 The tests performed using the LAPD were motivated by the need to reduce costs associated
 22 with the construction of an evacuable cryostat for future multi-kiloton detectors. The primary
 23 goal of the LAPD has been achieved using a three stage approach including a gaseous argon
 24 purge, followed by stages of gas and liquid recirculation. Measurements from purity monitors
 25 installed in the cryostat suggest that purities that allow for large electron drift lifetimes can be
 26 achieved in a large volume of liquid argon without first evacuating the vessel. In addition to
 27 demonstrating that evacuation is not necessary for achieving long electron lifetimes, we studied
 28 temperature gradients, the liquid argon volume exchange rates, filter loading capacity, and the
 29 effect of introducing other materials into the cryostat.

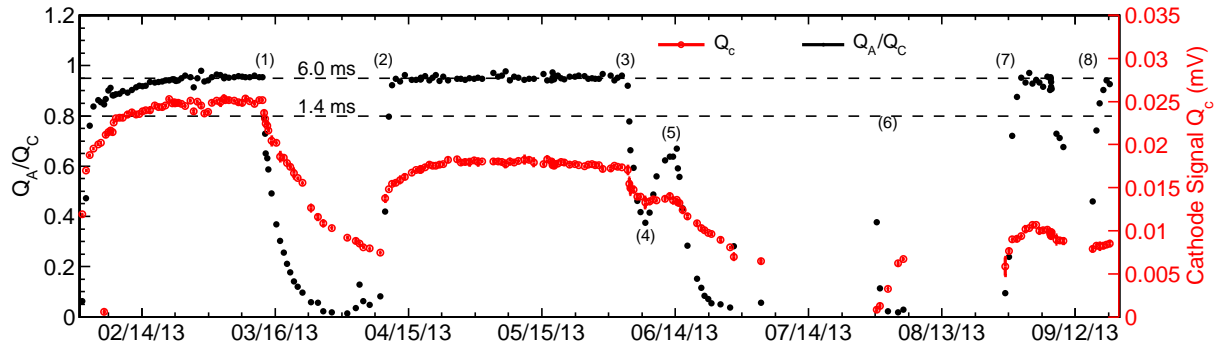


Figure 22. The cathode signal (Q_C) indicated as open red circles and the anode-to-cathode ratio (Q_A/Q_C) indicated as solid black circles for recirculated liquid argon over all LAPD running. The anode-to-cathode ratio is correlated with electron lifetime, calculated at values of 0.95 and 0.8. Gaps in the data occur when either the purity monitors do not have sufficient resolving power or when they were not operating. Special events are enumerated with the following descriptions: (1) Circulation pump trip for an extended time period. (2) Beginning of contamination cleanup, see Figure 20a). (3) Pump trip lasting one hour resulting in subsequent zero flow to the filters (4) Start of flow to filters after the pump trip. (5) Stopped pump for removal and repair (6) Start of second cleanup, see Figure 20b). (7) Start of third cleanup, see Figure 20c). (8) Pump restart after a few-day period to insert a digital camera.

1

2 Acknowledgments

3

4 We thank the staff at FNAL for their technical assistance in running the LAPD experiment. We
5 acknowledge support by the Grants Agencies of the DOE.

6 **REFERENCES**

- 7 1. J. N. Marx and D. R. Nygren, *Phys. Today* **31N10**, 46 (1978).
8 2. E. Gatti *et al.*, *IEEE Trans. Nucl. Sci.* **26**, 2910 (1979).
9 3. T. Akiri *et al.* (LBNE Collaboration), arXiv:1110.6249 [hep-ex].
10 4. C. Rubbia, *et al.*, *Journal of Instrumentation*, **6** P07011 (2011).
11 5. S. Amerio *et al.*, *Nucl. Instrum. Meth. A* **527**, 329 (2004).
12 6. R. Andrews *et al.*, *Nucl. Instrum. Meth. A* **608**, 251 (2009).
13 7. C. Anderson, *et al.* *Journal of Instrumentation*, **7**, P10019 (2012).
14 8. A. Ereditato, *et al.*, *Journal of Instrumentation*, **8**, P7002 (2013).
15 9. R. Schmitt, Presented at the Cryogenic Liquid Detectors for Future Particle Physics Work-
16 shop at LNGS, (2006).
17 10. W. Jaskierny *et al.*, FERMILAB-TM-2384-E.
18 11. Siemens Corp., Siemens Aktiengesellschaft, Wittelsbacherplatz 2, 80333 Munich Germany.
19 12. GE Intelligent Platforms, 2500 Austin Drive, Charlottesville, VA 22911 USA.
20 13. Automation Direct Inc., 3505 Hutchinson Road, Cumming, GA 30040 USA.
21 14. Sigma-Aldrich, P.O. Box 14508, St. Louis, MO 63178 USA.
22 15. BASF Corp., 100 Park Avenue, Florham Park, NJ 07932 USA.

- 1 16. Aspen Aerogels, Inc., 30 Forbes Road, Building B, Northborough, MA 01532 USA.
- 2 17. Barber-Nichols Inc., 6325 West 55th Avenue, Arvada, CO 80002 USA.
- 3 18. Micro Motion, Inc., 7070 Winchester Circle, Boulder, CO 80301 USA.
- 4 19. Platypus Technologies, LLC, Madison, WI USA.
- 5 20. Newport Corp., 1791 Deere Avenue, Irvine, CA 92606 USA.
- 6 21. Polymicro Technologies, 18019 N 25th Ave, Phoenix, AZ 85023 USA.
- 7 22. Tektronix Inc., 14200 SW Karl Braun Drive, Portland, OR 97077 USA.
- 8 23. B. Rebel *et al.*, J. Phys. Conf. Ser. **308**, 012023 (2011).
- 9 24. G. Carugno *et al.*, Nucl. Instrum. Meth. A **292**, 580 (1990).
- 10 25. O. Bunneman, B. Cranshaw and J.A. Harvey, Can J. Res. **27**, 191 (1949)
- 11 26. E. Voirin, LAPD Cryostat Interior temperatures-RTD measurements and CFD models of
- 12 Liquid and Gas Temperatures, LARTPC-doc-635-v4, 5/13/2013